Scattering-dominated high-temperature phase of 1T−TiSe2 : An optical conductivity study

Velebit, Kristijan; Popčević, Petar; Batistić, Ivo; Eichler, M.; Berger, H.; Forró, L.; Dressel, M.; Barišić, Neven; Tutiš, Eduard

Journal article, Published version
Rad u časopisu, Objavljena verzija rada (izdavačev PDF)

Permanent link / Trajna poveznica: https://urn.nsk.hr/urn:nbn:hr:217:154374

Download date / Datum preuzimanja: **2025-01-31**

Repository / Repozitorij:

Repository of the Faculty of Science - University of Zagreb

Scattering-dominated high-temperature phase of 1T-TiSe₂: An optical conductivity study

K. Velebit,[1,2] P. Popčević,[1,3] I. Batistić,[4] M. Eichler,[2] H. Berger,[5] L. Forró,[5] M. Dressel,[2] N. Barišić,[1,2,3] and E. Tutiš[1,*]

[1]*Institute of Physics, Bijenička c. 46, HR-10000 Zagreb, Croatia*
[2]*1. Physikalisches Institut, Universität Stuttgart, Pfaffenwaldring 57, 70569 Stuttgart, Germany*
[3]*Institute of Solid State Physics, Vienna University of Technology, 1040 Vienna, Austria*
[4]*Department of Physics, Faculty of Science, University of Zagreb, Bijenička c. 32, HR-10000 Zagreb, Croatia*
[5]*Ecole Polytechnique Fédérale de Lausanne, LPMC, CH-1015 Lausanne, Switzerland*

The controversy regarding the precise nature of the high-temperature phase of 1T-TiSe₂ lasts for decades. It has intensified in recent times when new evidence for the excitonic origin of the low-temperature charge-density wave state started to unveil. Here we address the problem of the high-temperature phase through precise measurements and detailed analysis of the optical response of 1T-TiSe₂ single crystals. The separate responses of electron and hole subsystems are identified and followed in temperature. We show that neither semiconductor nor semimetal pictures can be applied in their generic forms as the scattering for both types of carriers is in the vicinity of the Ioffe-Regel limit with decay rates being comparable to or larger than the offsets of band extrema. The nonmetallic temperature dependence of transport properties comes from the anomalous temperature dependence of scattering rates. Near the transition temperature the heavy electrons and the light holes contribute equally to the conductivity; this surprising coincidence is regarded as the consequence of dominant intervalley scattering that precedes the transition. The low-frequency peak in the optical spectra is identified and attributed to the critical softening of the L-point collective mode.

I. INTRODUCTION

In the continuing search for new collective electronic states, layered materials repeatedly appear as valuable sources and inspiration [1–5]. Transition-metal dichalcogenides (TMDs) have been among the earliest families of quasi-two-dimensional (2D) materials to host the quest, and they continue to provide surprises and puzzles [1,3,6–8]. 1T-TiSe₂ was one of the first TMDs from the IVb group where the charge-density wave (CDW) ordering was identified, yet the mechanism behind the transition has been debated ever since [1,9–11]. Front contenders for the explanation of the CDW ordering in 1T-TiSe₂ are the long-sought "excitonic insulator" and the indirect band Jahn-Teller mechanism [1,3,12–16] with the relative importance of electron-electron and electron-phonon interactions still being disputed [14,17–20]. The whole development has further emphasized the need to understand the nature of the high-temperature state that gives birth to the CDW phase. From early to recent times, the question has been reoccurring if this state is a semimetal or a semiconductor [14,21–24]. The reports range from a semiconductor with a finite indirect gap up to 150 meV [14,22] to a semimetal with an indirect band overlap up to 120 meV [23,24]. Understandably, a firm grasp of the high-temperature state is required for the proper understanding of the mechanism of the CDW transition. Two opposing pictures relate to two very different views on transport in the high-temperature phase: The observed nonmetallic temperature dependence of resistivity may be regarded as the consequence of the variation of the carrier density with temperature or as the result of the anomalous temperature dependence of the scattering rate. The two mechanisms also reflect very differently in the temperature

dependence of the Hall coefficient where the compensation of electron and hole contributions opens an additional window into the process.

This paper aims to answer some of these pressing questions in 1T-TiSe₂. Our investigation is based on measuring and analyzing the optical response of the material at the temperatures above the CDW transition [25]. We combine the result of optical and dc transport measurements to identify the contributions of electron and hole subsystems to the low-frequency response and to the transport properties by resolving their respective spectral weights, scattering rates, and mobilities. We find that the carrier density is quasiconstant in temperature, whereas the scattering rates for electrons and holes change in temperature, going beyond the Ioffe-Regel limit. The energy scale $\hbar/\tau$ related to scattering is on the order of the absolute values of the gap (or indirect band overlap) previously quoted, rendering the question of precise bare bands offset less relevant. Instead, the strong-scattering regime points to the distinct possibility of dynamically shaped band edges.

II. THE MATERIAL AND EXPERIMENTAL DETAILS

1T-TiSe₂ is a quasi-2D layered material where each layer consists of one Ti plane sandwiched between two Se planes. The 1T polytype features one Ti atom in an octahedral arrangement between six Se atoms. In the high-temperature phase the material has a hexagonal structure. All theoretical and experimental papers, including electronic structure calculations and angle-resolved photoemission spectroscopy (ARPES) experiments, agree that the conduction-band minimum (at the L point in the Brillouin zone) and the valence-band maximum (at the Γ point) are close in energy [14,22,24–27]. These two bands have very different dispersions near the Fermi level with the effective masses as measured in ARPES and concurred by density functional theory calculations being an
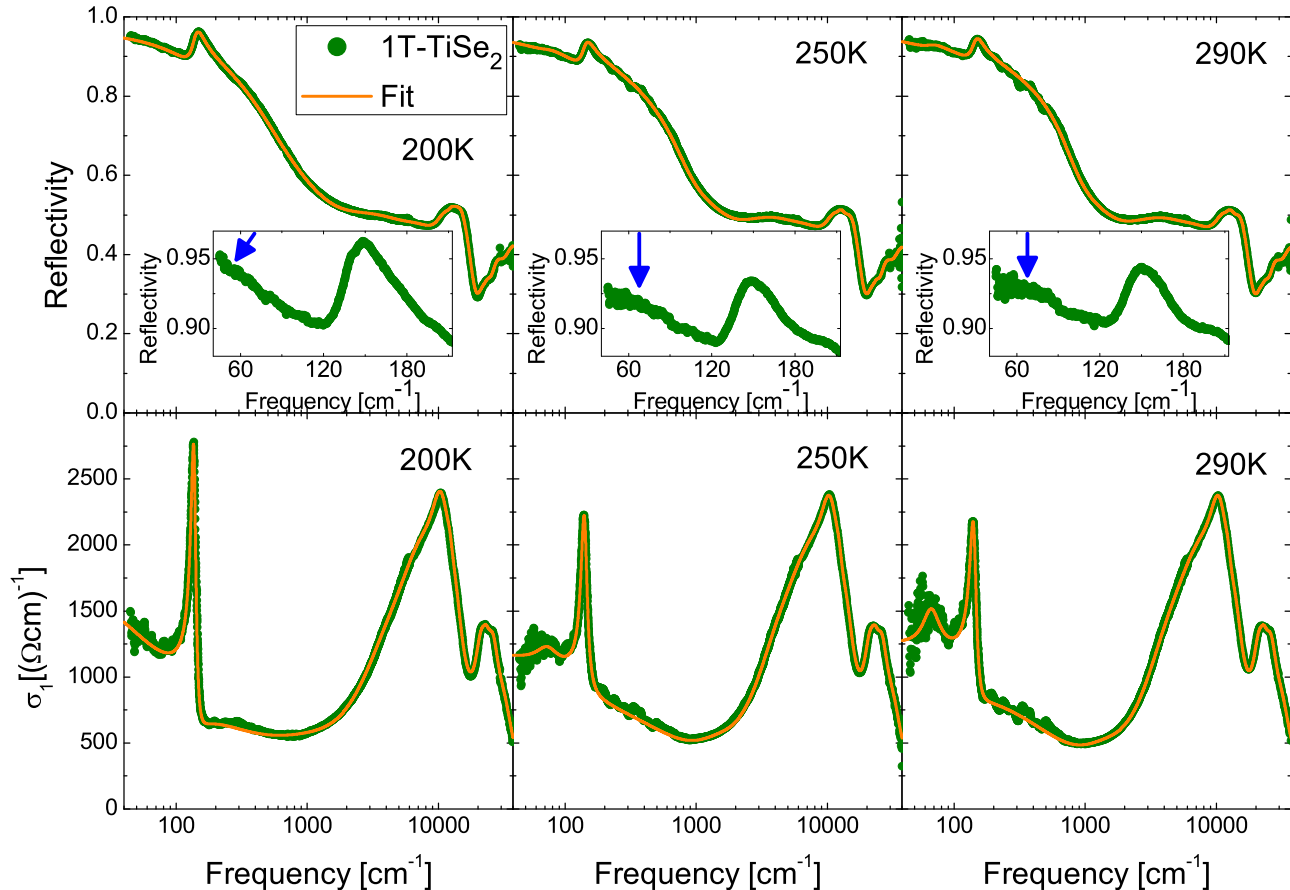
FIG. 1. Experimental data for reflectivity and optical conductivity of $1T$-TiSe$_2$ in the high-temperature phase $200\,\mathrm{K} \leqslant T \leqslant 290\,\mathrm{K}$ in the frequency window from 40 to $37\,000\,\mathrm{cm}^{-1}$ (note the logarithmic scale on the horizontal axis). The full lines on top of the data represent the Kramers-Kronig-consistent fits as elaborated in the text. The insets in the upper panels show the reflectivity below $200\,\mathrm{cm}^{-1}$. The arrows in the insets point to the low-frequency mode discussed in Sec. III (the arrow points to the frequency ω_{LF} on the horizontal axis).

order of magnitude bigger in the conduction band than in the valence band. Around 200 K (T_{CDW}) the material undergoes the second-order phase transition to the commensurate charge-density wave state [9]. The rise of the $2 \times 2 \times 2$ superstructure involves the softening of a phonon at the high-symmetry L point of the Brillouin zone [28–30]. The electrical resistivity $\rho(T)$ exhibits the peak in $d\rho(T)/dT$ around T_{CDW} associated with the superlattice formation followed by the maximum in $\rho(T)$ near 165 K [9,10,31]. At room temperature the Hall coefficient R_H is positive, indicating that holes are more mobile than electrons in the high-temperature phase but falls to zero near the transition temperature, indicating complete compensation of electron and hole contributions to the Hall signal [10].

The single-crystal $1T$-TiSe$_2$ samples used in this study were grown by a conventional chemical vapor transport method. The typical size of the crystal samples was $3 \times 2 \times 0.5\,\mathrm{mm}^3$. We measured the optical reflectivity (planar response) of $1T$-TiSe$_2$ in the temperature range between 200 and 290 K and a broad frequency range from 40 to $37\,000\,\mathrm{cm}^{-1}$. A Bruker IFS 113v was used for the far-infrared measurements ($40 - 800\,\mathrm{cm}^{-1}$), gold was evaporated onto the sample *in situ*, and reference measurements were performed at each measured temperature. The mid-infrared range was measured with a Bruker Vertex 80v equipped with a HYPERION IR

microscope, and freshly evaporated aluminum mirrors were used as a reference. A Woolam variable-angle spectroscopic ellipsometer was used for the near-infrared to ultraviolet frequency range. The measurements were performed in vacuum. This procedure greatly increases the precision of the low-frequency measurements and the outcome of the Kramers-Kronig (KK) transformation, particularly regarding the relative changes that occur with the change in temperature. The measurements were performed at 200, 225, 250, and 290 K.

III. EXPERIMENTAL RESULTS AND ANALYSIS

The experimental results for reflectivity $R(\omega)$ are shown in Fig. 1, along with the real part of optical conductivity $\sigma_1(\omega)$, as obtained using the KK transformation [32–34]. Figure 1 also shows the curves that are the results of the modeling to be discussed below. The minimum in optical conductivity occurs around $1000\,\mathrm{cm}^{-1}$. This frequency roughly separates the parts of the spectra dominated by contributions of intra- and interband processes.

There are several hints about the nontrivial nature of the high-temperature phase that may be obtained already at the level of raw data. The first hint comes from Fig. 2 which shows the temperature dependence of the partial spectral weight
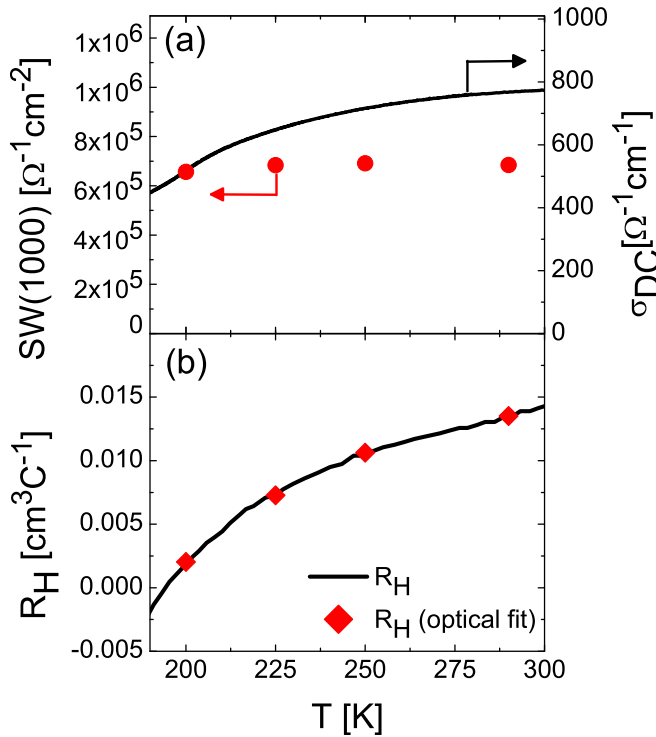
FIG. 2. (a) The comparison of the temperature dependence of dc conductivity $\sigma_{dc}(T)$ and the partial spectral weight $SW(1000) \equiv \int_a^b \sigma_1(\omega)d\omega$, $a = 40$, $b = 1000\,\mathrm{cm}^{-1}$. The nonmetallic increase in conductivity with increasing temperature is not accompanied by any comparable change in the spectral weight. (b) Similarly, the temperature dependence of the Hall coefficient does not reflect the temperature dependence of the carrier density in a generic stoichiometric semiconductor. The figure shows the points that correspond to optical fits in Fig. 1 on the top of the measured Hall coefficient from Ref. [10].

$SW(1000) \equiv \int_a^b \sigma_1(\omega)d\omega$, where $a = 40$ and $b = 1000\,\mathrm{cm}^{-1}$ related to the frequency window that extends from the lowest measured frequency up to the crossover at $1000\,\mathrm{cm}^{-1}$. This spectral weight shows no significant variation in temperature. This supports the viewpoint, expressed in some previous papers, of the semimetallic nature of $1T$-TiSe₂ [23,24]. Accordingly, the sizable nonmetallic change in conductivity in the same temperature range may not be ascribed to the variation of the carrier density in temperature, usual for semiconductors.

The second hint comes from the value of the dc conductivity also shown in Fig. 2. Using the value $d_\perp \approx 6\text{Å}$ for the separation between TiSe₂ layers, one calculates the conductance per sheet $\sigma_{dc}d_\perp$. This turns out to be on the order of conductance quantum $G_0 = 2e^2/h \approx 7.75 \times 10^{-5}\,\Omega^{-1}$. Meeting this limit in a two-dimensional metal ordinarily means that the strong-scattering limit is reached with the mean-free path being on the order of inverse Fermi wave vector $\ell \sim k_F^{-1}$. For a quasi-two-dimensional semimetal with a finite overlap of conduction and valence bands this also implies that all states in the energy range of band overlap are strongly affected by scattering. The latter point will be further detailed in Sec. III.

These hints being noted, it may be rightly claimed that $1T$-TiSe₂ is not a simple 2D metal, whereas the quantity SW(1000) shown in Fig. 2 is based on a sharp and somewhat arbitrary cutoff frequency. A meticulous analysis of the spectra is called upon, and this is what we aim to provide in the following paragraphs.

This analysis must also observe the multicarrier nature of transport in $1T$-TiSe₂, witnessed by the Hall coefficient, shown in Fig. 2(b). The temperature dependence of the Hall coefficient as noted previously in Ref. [10] primarily reflects the dependence of mobility on temperature and the fact that mobilities of electrons (μ_h) and holes (μ_e) get equal near the transition point. This observation is based on the fact that concentrations of electrons and holes are equal in the stoichiometric compound $n_h = n_e = n$, simplifying the textbook formula for the Hall coefficient [10,35,36],

$$R_H = \frac{1}{e}\frac{n_h\mu_h^2 - n_e\mu_e^2}{(n_h\mu_h + n_e\mu_e)^2} = \frac{1}{ne}\frac{1 - \frac{\mu_e}{\mu_h}}{1 + \frac{\mu_e}{\mu_h}}. \quad (1)$$

Having comparable mobilities and the same concentrations for holes and electrons also implies that their contributions to dc conductivity $\sigma_{dc,h}$ and $\sigma_{dc,e}$ are comparable and get precisely equal in the proximity of the transition point where R_H vanishes [10]. This may appear as a surprising coincidence, given the order of magnitude difference in effective masses found for the two bands. In other words, the scattering rate for lighter carriers (holes) must be an order of magnitude bigger than the scattering rate of heavier carriers (electrons). This great difference in scattering rates for the two channels that contribute comparably in the dc limit is expected to show in optical data as well. Indeed, several authors have already noted that the low-frequency electronic response may not be described by a single Drude term [23,37]. It may be expected that several Drude terms are required in the minimal model for the low-frequency optical response in $1T$-TiSe₂ as in some other multiband systems [38–40].

The modeling of the optical response, to be presented below, is always performed in the KK-consistent manner, i.e., by validating the model against reflectivity and conductivity data sets. The overall fits that emerge are shown in Fig. 1 as full lines on the top of the data [41]. The straightforward approach to modeling of complex optical conductivity $\sigma(\omega) = \sigma_1(\omega) + i\sigma_2(\omega)$ proceeds by separating the contributions of electrons and phonons $\sigma(\omega) = \sigma_{el}(\omega) + \sigma_{phon}(\omega)$. It is convenient to start with phonons since this part of the spectrum is very simple in the high-temperature phase of $1T$-TiSe₂, consisting of a single infrared-active phonon mode ("Se mode") at a frequency somewhat above $130\,\mathrm{cm}^{-1}$ [23,42,43]. Also, compared to all other signals, this mode is very narrow in frequency, which makes it easier to parametrize and separate its contribution from the others. This separation is easy to perform despite pronounced Fano-type asymmetry which signals the coupling of the phonon to the electronic continuum. The well-known Fano formula $\sigma_{phon}(\omega) = \varepsilon_0\omega S_0^2(1 - \frac{i}{q_0})^2[i(\omega_0^2 - \omega^2) + \omega\gamma_0]^{-1}$ is used to parametrize the contribution [44–47]. Figure 3 illustrates how it appears in the full spectrum decomposition at 250 K.
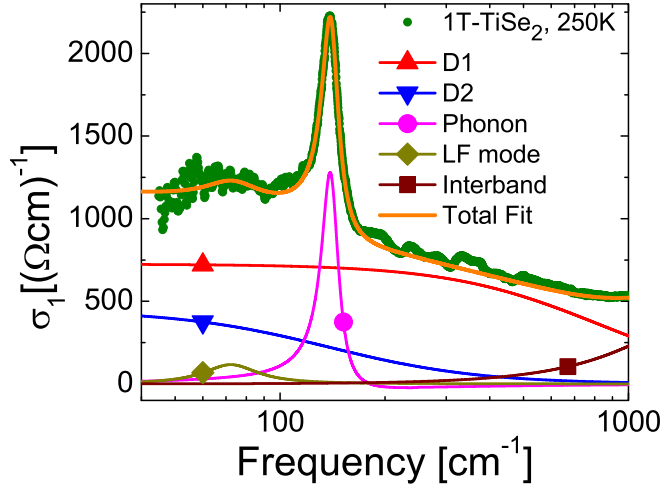
FIG. 3. The real part of the optical conductivity of $1T$-TiSe$_2$ below $1000\,\mathrm{cm}^{-1}$ at 250 K along with the decomposition into components as discussed in the text. The related decomposition for the imaginary part is provided in the Supplemental Material [48].

As usual, the electronic part is parametrized by the Drude-Lorentz model,

$$\frac{\sigma_{\mathrm{el}}(\omega)}{\varepsilon_0} = \sum_j \frac{\omega_{p,Dj}^2}{\gamma_{Dj} - i\omega} + \sum_j \frac{\omega S_{Lj}^2}{i\left(\omega_{Lj}^2 - \omega^2\right) + \omega\gamma_{Lj}}, \quad (2)$$

with multiple Drude and Lorentz terms.

First we address the interband excitations that dominate the part of the spectrum above $1000\,\mathrm{cm}^{-1}$. Figure 1 shows precise fits to this part of the spectrum produced by using appropriate Lorentz terms [49]. As illustrated in Fig. 2, these terms also produce a weak and featureless tail in the frequency window below $1000\,\mathrm{cm}^{-1}$, which is the frequency range of our primary interest. Thus, apart from simulating the strength, the form, and the KK-consistent analytic structure of the interband contributions above $1000\,\mathrm{cm}^{-1}$, these Lorentz terms also serve to improve our analysis in the frequency region below $1000\,\mathrm{cm}^{-1}$. We also find that the temperature dependence of the interband contribution is small and negligible in comparison to the temperature dependence of the other parts of the spectrum [49].

At last, we turn to the frequency range below $1000\,\mathrm{cm}^{-1}$. We find that this part of the electronic response is very well described by the sum of two Drude contributions, parametrized by very different sets of parameters $(\omega_{p,D_1}, \gamma_{D_1})$ and $(\omega_{p,D_2}, \gamma_{D_2})$. Motivated by previous measurements of electronic spectra and band structure calculations we identify the two terms as responses of holes and electrons ($D_1 \equiv h$, $D_2 \equiv e$). These parameters are refined not only by producing the best possible fits to the optical data in Fig. 1, but also by obeying the constraints that arise from dc measurements. First, we take care that the relative change in optical conductivity in the $\omega \to 0$ limit $\sigma_1(\omega \to 0) = \varepsilon_0\omega_{p,e}^2/\gamma_e + \varepsilon_0\omega_{p,h}^2/\gamma_h$ follows the relative change in dc conductivity $\sigma_{\mathrm{dc}}(T)$. Second, we demand that the mobility ratio that we extract from these parameters $\mu_e/\mu_h = \omega_{p,e}^2\gamma_h/\omega_{p,h}^2\lambda_e$ is consistent with measured temperature dependence of the Hall coefficient through Eq. (1). This requires that the mobility ratio approaches unity around 200 K as well
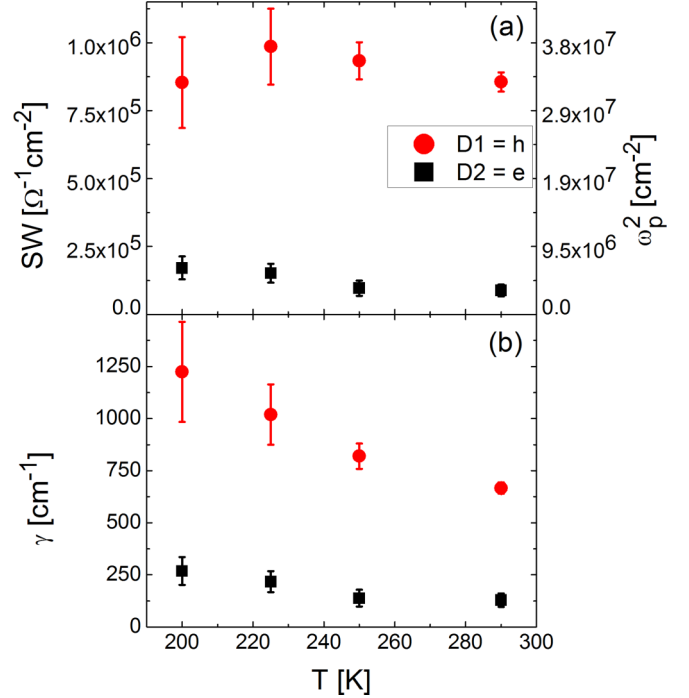

FIG. 4. The results of the Kramers-Kronig-consistent fit to the experimental optical data of $1T$-TiSe$_2$ in the high-temperature phase $(290\,\mathrm{K} \geqslant T \geqslant 200\,\mathrm{K})$. (a) Spectral weights of two Drude terms that model the electronic response below $1000\,\mathrm{cm}^{-1}$. SW is the spectral weight of the Drude term defined as $\mathrm{SW} = \pi\varepsilon_0\omega_p^2/2$, where ω_p is the plasma frequency. The right axis shows the square of the plasma frequency. (b) The quantity γ is the width (or damping) of the Drude term expressed in cm^{-1}, inversely proportional to the transport scattering time.

as that the temperature dependence of this ratio primarily accounts for $R_H(T)$ in Fig. 2(b). Naturally, one should also consider the temperature dependence of the carrier density n in Eq. (1). However, as already stated in relation to integral SW(1000) in Fig. 2(a), this dependence is not expected to be very pronounced. Thus we take the approach where we start with n being temperature independent and check the results for consistency. The value of $n = 1.4 \times 10^{20}\,\mathrm{cm}^{-3}$ is obtained by optimizing the fits in optical conductivity and reflectivity for all temperatures. This value comes within the factor of 2 of the original rough estimate made in Ref. [10] for the carrier density at room temperature, and no compensation effects are taken into account. The resulting parameters that characterize the optical response of electron and hole subsystems are shown in Fig. 4. Figure 4(a) shows the temperature dependence of spectral weights [32],

$$\mathrm{SW}_a \equiv \int_0^\infty d\omega\, \sigma_{1,a}(\omega) = \frac{\pi\varepsilon_0\omega_{p,a}^2}{2} = \frac{\pi n_a e^2}{2m_a^*}$$

$$= \frac{\pi n e^2}{2m_a^*} \quad (a = h,e), \quad (3)$$

proportional to the squares of respective plasma frequencies $\omega_{p,h,e}$, whereas the scattering rates $\gamma_{h,e}$ are shown in Fig. 4(b) [50]. The spectral weight for holes (SW$_h$) is weakly temperature dependent, the variation being on the order of error
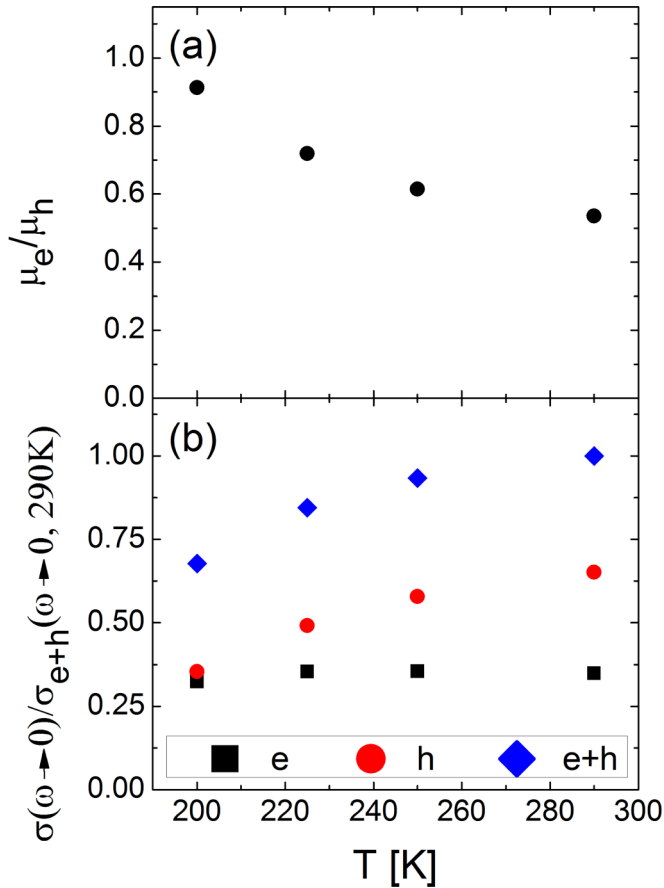
FIG. 5. (a) The temperature dependence of the ratio of electron and hole mobilities as inferred from optical conductivity below $1000 \, \text{cm}^{-1}$. (b) Contributions of electrons and holes to conductivity in the dc limit.

bars, consistent with the assumption of the carrier density n being weakly temperature dependent. The variation of the electronic spectral weight (SW_e) is also much smaller than the total spectral weight, although some rise in SW_e may be observed as the temperature is lowered. This rise is possibly related to the increased mixing of two bands upon lowering the temperature to be discussed further below. It may be further noticed that the ratio SW_h/SW_e obtained from our data in Fig. 4 comes very close to the value of $m_e/m_h \approx 9.65$ measured in ARPES at 260 K [14]. Also, the absolute values of effective masses using the spectral weights in Fig. 4 and the carrier density n are close to the values derived from ARPES data [14].

The temperature dependence of the mobility ratio is shown in Fig. 5(a). The electrons are less mobile than holes at room temperature, but μ_e/μ_h increases upon lowering the temperature and approaches unity around 200 K. Figure 5(b) gives the temperature dependence of electron and hole conductivities in the zero-frequency limit $\sigma_{h,e}(\omega \to 0) = (2/\pi)(\text{SW}_{h,e}/\gamma_{h,e})$.

Finally, we discuss the least pronounced feature of our low-frequency spectra, the low-frequency peak whose spectral weight is much smaller than the spectral weights of the Drude terms. The peak has a characteristic finite frequency ($\omega_{LF} \approx 69 \, \text{cm}^{-1}$ at 250 K), which is well below the Se-phonon
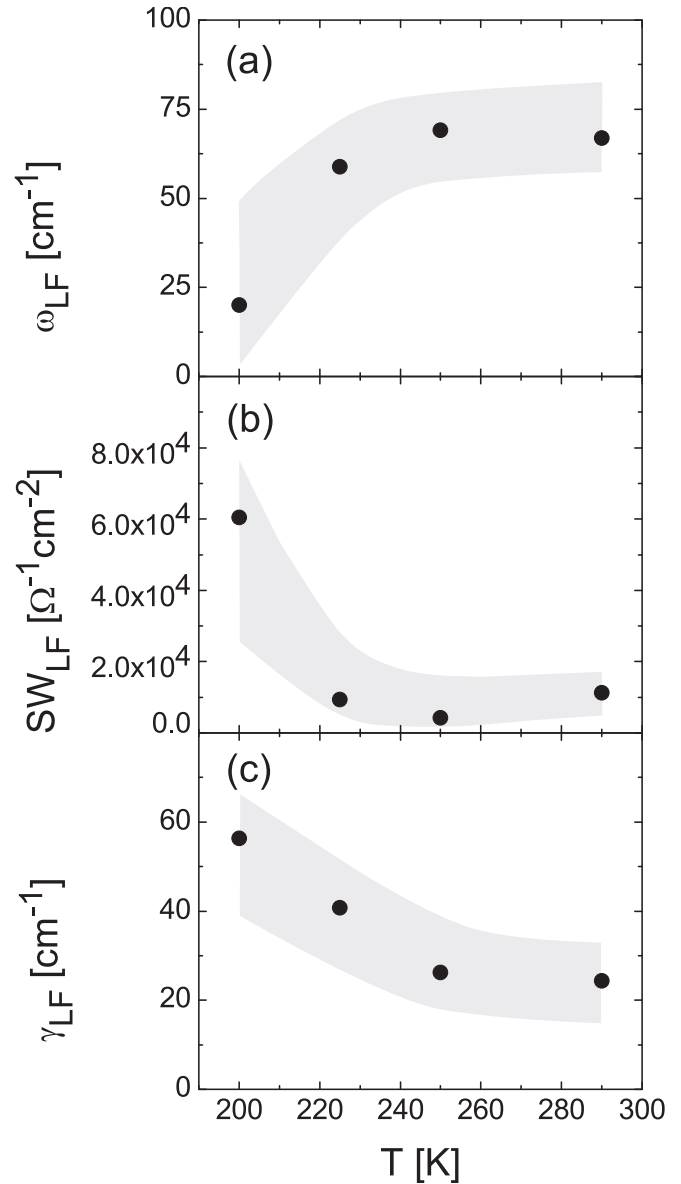

FIG. 6. Temperature dependence of the parameters of the low-frequency mode. As the temperature is lowered towards the transition temperature, the frequency of the mode lowers, whereas the damping and the spectral weight of the mode increase. The gray-shaded areas represent the confidence intervals for the parameters of the low-frequency mode, whereas the points represent the values of parameters used in Figs. 1 and 2.

mode frequency. The peak is considerably broader than the phonon mode but appears clearly visible as the step in the raw reflectivity data (insets in the top panels in Fig. 1). It is also visible in the optical conductivity, despite the experimental noise being very much amplified by the KK transformation (which is typical whenever reflectivity approaches unity). The low-frequency peak is parametrized by the Lorentz form with the parameters shown in Fig. 6 [51]. As a consequence of the noise, the KK-consistent fits yield significant error bars for the parameters. However, several features can be followed despite the noise and even observed in raw data: As the transition temperature is approached, the characteristic frequency of the

low-frequency mode ω_{LF} decreases, the spectral weight of the mode increases, and the damping γ_{LF} gets larger. Given the values and the temperature dependence of the parameters, it is clear that the observed mode cannot be related to any of the $q = 0$ phonon modes in the high-temperature phase of $1T$-TiSe$_2$. On the other hand, the frequency range and temperature dependence of the frequency $\omega_{LF}(T)$ resembles the softening of the phonon branch around the L point in the Brillouin zone (hereafter the "L-phonon mode"), observed through diffuse x-ray scattering above the transition temperature [28–30]. However, the phonon at the boundary of the Brillouin zone can be excited by light only if assisted by another excitation which provides the required crystal momentum. This excitation is easy to point to in $1T$-TiSe$_2$ as the very appearance of the Kohn anomaly reflects the coupling of the L-point phonon mode to the electronic interband excitations, involving the valence-band states near the Γ point and conduction-band states near the L point. This mixing of bands has been previously observed in ARPES at 260 K [14]. The process is illustrated in Fig. 7. In particular, the process of creation of a soft phonon by photons, assisted by the electronic quasielastic interband excitation, is depicted in Fig. 7(c). Alternatively, this process may be considered as (soft-)phonon-assisted interband excitation. Even more correctly, it should be regarded as the collective excitation in which phonon and electron-hole excitations are mixed and probably further amplified by the Coulomb (excitonic) correlations in the electron-hole channel [19,21,52].

IV. DISCUSSION

The picture of the semimetal carried so far may be examined further by comparing all the energy scales involved. First, the measured spectral weight SW$_h$ can be used to assess the energy span ΔE_h of states in the valence band required to host the holes in the absence of thermal smearing,

$$\Delta E_h = \frac{\hbar^2 k_{F,h}^2}{2m_h^*} = \frac{\hbar^2 \pi n_h d_\perp}{m_h^*} = \frac{2\hbar^2}{e^2} d_\perp \mathrm{SW}_h, \qquad (4)$$

where $k_{F,h}$ and $d_\perp$ denote the Fermi wave vector of the quasi-two-dimensional hole gas and the lattice constant in the direction perpendicular to the planes, respectively [46]. The value of $\Delta E_h/k_B$ thus obtained from data in Fig. 4(a) lies between 600 and 700 K, roughly three times the transition temperature. The same is not true for electrons. For similarly defined ΔE_e's the value obtained is approximately tenfold smaller, which implies that electrons in the conduction band are in the state of Drude gas $\Delta E_e \ll k_B T$ [53]. The total overlap of the conduction and valence bands may be estimated to (see Fig. 7) $\Delta E \approx \Delta E_h + \Delta E_e \approx \Delta E_h \approx 0.056(\pm 0.005)$ eV ($\Delta E/k_B \sim 650$ K).

On the other hand, the data for the scattering rates, shown in Fig. 4(b), yield $\hbar\gamma_h/k_B$ ranging from 960 K at room temperature to 1760 K around the transition temperature. The relation between bandwidth and scattering rate $\Delta E_h \lesssim \hbar\gamma_h$ reflects the strong-scattering regime announced in the Introduction, here quantified for the hole channel. A similar relation also holds for electrons in the conduction band since $(\Delta E_e/\gamma_e)/(\Delta E_h/\gamma_h) = \mu_e/\mu_h$ is on the order of unity. The overall relation that connects the six energy scales in $1T$-TiSe$_2$
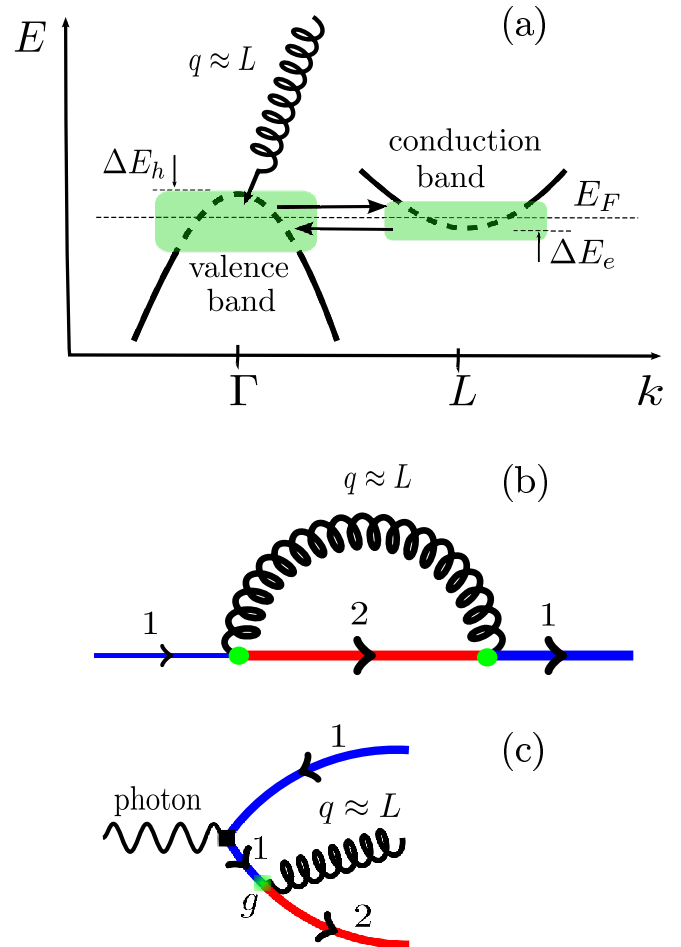

FIG. 7. (a) The schematic of the quasielastic interband scattering that involves the collective soft phonon/boson mode (coiled line) at $q \approx L$. The scattering strongly affects the electronic states near the band edges (shaded areas), which dominantly contribute to low-frequency optical response. (b) The self-energy diagram representing the same scattering process (lowest order of perturbation) related to Eq. (6). The indices 1 and 2 stand for states in the conduction and valence bands or vice versa; (c) The process of photon absorption that leads to the generation of a soft phonon/boson in the high-temperature phase related to the observed low-frequency mode. The process is assisted by the quasielastic interband electron excitation.

in the observed temperature range is

$$\Delta E_e \leqslant k_B T \sim \hbar\gamma_e \ll \Delta E_h \approx \Delta E \leqslant \hbar\gamma_h. \qquad (5)$$

Obviously, strong carrier scattering, above the Ioffe-Regel limit $\Delta E_h \sim \hbar\gamma_h$, $\Delta E_e \sim \hbar\gamma_e$, is the essential property of the high-temperature phase of $1T$-TiSe$_2$. It is possible that this scattering appears as a wide precursor of the CDW phase, involving the mode at $q \approx L$ that softens throughout the temperature range addressed here [21,28]. Figures 7(a) and 7(b) which illustrate the process also suggest the mechanism in which this scattering acts to equalize the mobilities of the carriers in these two bands: The carriers in the valence band are scattered into the conduction band and vice versa. Of course, in both cases the scattering rates are determined by the density of final states. Therefore, the scattering rate of the lighter carrier type is proportional to the band mass of the heavier one and

vice versa $\gamma_h \propto g^2 m_e$ and $\gamma_e \propto g^2 m_h$ [g denotes the relevant electron-phonon coupling, pictured as bullets in Figs. 6(b) and 6(c)]. This leads to two mobilities being comparable,

$$\mu_h \approx A \frac{1/\gamma_h}{m_h} = A' \frac{1}{m_h g^2 m_e} = A \frac{1/\gamma_e}{m_e} \approx \mu_e, \quad (6)$$

when this type of scattering process becomes dominant. The proportionality factors A and A' that contain some less interesting factors are introduced for convenience [54]. This may explain the observed tendency of two mobilities becoming close in value as the transition point is approached and the scattering being increased. Thus the compensation that occurs by having the lighter type of carriers heavily scattered and vice versa is likely nonaccidental. It must be emphasized, however, that the diagram in Fig. 7(b) and relation (6) represent the interpocket scattering process to its lowest order, whereas the full solution of the (strong) quasistatic scattering problem and related transport is still pending.

In this respect, we would like to add a comment regarding the running "semimetal vs semiconductor" dichotomy, mostly spanned by optical and ARPES studies. First, it should be emphasized that the large scattering rate found here is not at odds with ARPES data where the electronic spectra in the high-temperature phase show substantial smearing near the band edges. In fact, it has been proposed recently by the authors involved in ARPES and theoretical modeling that the low-frequency optical response in $1T$-TiSe$_2$ is due to carriers that occupy the long spectral tails of the single-particle spectral functions [21]. Our findings confirm that strong scattering is the primary feature of the electronic response and probably the root of the dichotomy. It must be kept in mind, however, that beyond smearing of the quasiparticle states over some energy range $\hbar\gamma$, scattering is likely to reshape the electronic dispersion on the same energy scale. This is best viewed in quasi-one-dimensional Peierls systems which have been intensely studied for decades and where the CDW transition is also announced by the development of the (Kohn) anomaly in the phonon spectrum, often over an extended temperature range. These systems bear a strong resemblance as well as some important differences with respect to $1T$-TiSe$_2$. For comparison, the nonmetallic resistivity behavior in some of these systems extends very much above the CDW ordering temperature [55–57]. The ARPES studies in the same temperature range have revealed largely suppressed density of states at the Fermi level—the "pseudogap" state, sometimes ascribed to the (bi)polaronic redistribution of the quasiparticle spectral weight away from the Fermi level [56,58,59]. Moreover, similar to our findings in $1T$-TiSe$_2$, the optical studies in the same temperature range find finite "Drude-type" signals with large widths that indicate strong scattering as well as the "collective mode," which resembles our low-frequency mode [59–62]. Conversely, to the ongoing controversy about the ultimate high-temperature starting point in $1T$-TiSe$_2$, the starting point for the Peierls mechanism is undoubtedly the metallic state with the Fermi level positioned deeply within the band. Despite that, the observed electronic spectra very much deviate from this simple picture in the wide temperature range above the transition, suggesting that strong scattering processes are responsible for the formation of the pseudogap state. The non-

perturbative approach required to capture this effect in the strong-scattering limit beyond the noncrossing approximation has been developed for single-band chain systems [63,64] but still awaited for materials, such as $1T$-TiSe$_2$.

V. CONCLUSIONS AND OUTLOOK

We have presented a comprehensive study of the high-temperature state of $1T$-TiSe$_2$ in which the optical spectral weights, scattering rates, and mobilities for electrons and holes are separately identified and followed in temperature. The study reveals the origin of the nonmetallic temperature dependence of the resistivity in a wide temperature range above the transition. The temperature behavior of the measured spectral weight rules out the simple explanation of this behavior as a consequence of the semiconductorlike state. Our data and our Kramers-Kronig-consistent analysis favor the picture of the high-temperature phase $1T$-TiSe$_2$ being a semimetal with the band overlap which is roughly three times the transition temperature. The temperature variation of the hole- and electron-scattering rates is responsible for the observed nonmetallic temperature dependence of dc resistivity as well as for the temperature dependence of the Hall coefficient. The difference in electron- and hole-scattering rates compensates the big difference in respective band masses, leading to comparable hole and electron contributions to the dc conductivity and their complete cancellation in the Hall coefficient in the proximity of the transition temperature. We argue that this behavior is the consequence of the strong interband quasielastic scattering in the CDW precursor regime.

On the other hand, our analysis also shows that both types of carriers are strongly scattered. The scattering energy scale goes beyond the previously quoted values for the gap, pointing to the possibility that band edges are primarily shaped by quasi-elastic-scattering processes. At this point it is of interest to consider the analogy to some strongly coupled Peierls system, which shares several common features with $1T$-TiSe$_2$, and where strong carrier scattering and the pseudogap state have been documented in a wide temperature range above the transition. All differences among the systems being acknowledged, the strong scattering, and the dynamical band reconstruction around the Fermi level may be the origin of the ongoing semimetal vs semiconductor controversy in $1T$-TiSe$_2$. Along with the previously observed shadow bands in ARPES, the low-frequency mode reported here may be regarded as another special manifestation of this state.

Admittedly, the low-frequency mode deserves more attention in future studies. It would be also interesting to extend the present study to doped materials. The cross comparison of optical, photoemission, and dc transport experiments on crystals from the same batch would be especially desirable.

ACKNOWLEDGMENTS

---

[1] J. A. Wilson and A. D. Yoffe, Adv. Phys. **18**, 193 (1969).

[2] J. G. Bednorz and K. A. Mueller, Z. Phys. B: Condens. Matter **64**, 189 (1986).

[3] R. H. Friend and A. D. Yoffe, Adv. Phys. **36**, 1 (1987).

[4] J. M. Williams, A. J. Schultz, U. Geiser, K. D. Carlson, A. M. Kini, H. H. Wang, W.-K. Kwok, M.-H. Whangbo, and J. E. Schirber, Science **252**, 1501 (1991).

[5] Y. Kamihara, H. Hiramatsu, M. Hirano, R. Kawamura, H. Yanagi, T. Kamiya, and H. Hosono, J. Am. Chem. Soc. **128**, 10012 (2006).

[6] E. Morosan, H. W. Zandbergen, B. S. Dennis, J. W. G. Bos, Y. Onose, T. Klimczuk, A. P. Ramirez, N. P. Ong, and R. J. Cava, Nat. Phys. **2**, 544 (2006).

[7] B. Sipos, A. F. Kusmartseva, A. Akrap, H. Berger, L. Forró, and E. Tutiš, Nature Mater. **7**, 960 (2008).

[8] Q. H. Wang, K. Kalantar-Zadeh, A. Kis, J. N. Coleman, and M. S. Strano, Nat. Nanotechnol. **7**, 699 (2012).

[9] F. J. Di Salvo, D. E. Moncton, and J. V. Waszczak, Phys. Rev. B **14**, 4321 (1976).

[10] F. J. Di Salvo and J. V. Waszczak, Phys. Rev. B **17**, 3801 (1978).

[11] D. L. Greenaway and R. Nitsche, J. Phys. Chem. Solids **26**, 1445 (1965).

[12] D. Jerome, T. M. Rice, and W. Kohn, Phys. Rev. **158**, 462 (1967).

[13] M. M. May, C. Brabetz, C. Janowitz, and R. Manzke, Phys. Rev. Lett. **107**, 176405 (2011).

[14] T. E. Kidd, T. Miller, M. Y. Chou, and T.-C. Chiang, Phys. Rev. Lett. **88**, 226402 (2002).

[15] K. Rossnagel, L. Kipp, and M. Skibowski, Phys. Rev. B **65**, 235101 (2002).

[16] R. S. Knox, in *Theory of Excitons, Solid-State Physics*, edited by F. Seitz and D. Turnbull (Academic, New York, 1963), Suppl. 5, p. 100.

[17] C. Monney, G. Monney, P. Aebi, and H. Beck, Phys. Rev. B **85**, 235150 (2012).

[18] S. Hellmann, T. Rohwer, M. Kalläne, K. Hanff, C. Sohrt, A. Stange, A. Carr, M. M. Murnane, H. C. Kapteyn, L. Kipp, M. Bauer, and K. Rossnagel, Nat. Commun. **3**, 1069 (2012).

[19] M. Porer, U. Leierseder, J.-M. Ménard, H. Dachraoui, L. Mouchliadis, I. E. Perakis, U. Heinzmann, J. Demsar, K. Rossnagel, and R. Huber, Nature (London) **13**, 857 (2014).

[20] More recently the superconductivity has been found in this material with superconducting domes appearing in a unique doping-pressure-temperature phase diagram next to the CDW phase [6,65]. The domes resemble those found in cuprate high-temperature superconductors and several other strongly correlated electron systems, although bordering phases in $1T$-TiSe$_2$ are unlike any of those found in other materials.

[21] G. Monney, C. Monney, B. Hildebrand, P. Aebi, and H. Beck, Phys. Rev. Lett. **114**, 086402 (2015).

[22] J. C. E. Rasch, T. Stemmler, B. Müller, L. Dudy, and R. Manzke, Phys. Rev. Lett. **101**, 237602 (2008).

[23] G. Li, W. Z. Hu, D. Qian, D. Hsieh, M. Z. Hasan, E. Morosan, R. J. Cava, and N. L. Wang, Phys. Rev. Lett. **99**, 027404 (2007).

[24] O. Anderson, R. Manzke, and M. Skibowski, Phys. Rev. Lett. **55**, 2188 (1985).

[25] Although there were previous investigations into the optical properties of $1T$-TiSe$_2$ [23], not much attention was given to the low-frequency response of the high-temperature phase.

[26] T. Rohwer *et al.*, Nature (London) **471**, 490 (2011).

[27] H. Cercellier, C. Monney, F. Clerc, C. Battaglia, L. Despont, M. G. Garnier, H. Beck, P. Aebi, L. Patthey, H. Berger, and L. Forró, Phys. Rev. Lett. **99**, 146403 (2007).

[28] M. Holt, P. Zschack, H. Hong, M. Y. Chou, and T.-C. Chiang, Phys. Rev. Lett. **86**, 3799 (2001).

[29] H. Barath, M. Kim, J. F. Karpus, S. L. Cooper, P. Abbamonte, E. Fradkin, E. Morosan, and R. J. Cava, Phys. Rev. Lett. **100**, 106402 (2008).

[30] F. Weber, S. Rosenkranz, J.-P. Castellan, R. Osborn, G. Karapetrov, R. Hott, R. Heid, K.-P. Bohnen, and A. Alatas, Phys. Rev. Lett. **107**, 266401 (2011).

[31] J. A. Benda, Phys. Rev. B **10**, 1409 (1974).

[32] M. Dressel and G. Grüner, *Electrodynamics of Solids: Optical Properties of Electrons in Matter* (Cambridge University Press, Cambridge, UK, 2003).

[33] C. Kittel, *Introduction to Solid State Physics*, 7th ed. (Wiley, New York, 1996).

[34] L. D. Landau and E. M. Lifshitz, *Electrodynamics of Continuous Media* (Addison-Wesley, Reading, MA, 1960).

[35] J. M. Ziman, *Electrons and Phonons* (Oxford University Press, Oxford, 1960), reprinted (2004).

[36] This is not affected by the fact that three equivalent electronic pockets exist in $1T$-TiSe$_2$. The contributions from three pockets simply add, and resulting n_e stands for the total density of electrons in the three pockets. Regarding the anisotropy of the conduction band in the vicinity of the L points, the effective electronic mass is expected to be dominated by the lightest mass as usual.

[37] H. P. Vaterlaus and F. Lévy, J. Phys. C: Solid State Phys. **18**, 2351 (1985).

[38] D. Wu, N. Barišić, P. Kallina, A. Faridian, B. Gorshunov, N. Drichko, L. J. Li, X. Lin, G. H. Cao, Z. A. Xu, N. L. Wang, and M. Dressel, Phys. Rev. B **81**, 100512(R) (2010).

[39] N. Barišić, D. Wu, M. Dressel, L. J. Li, G. H. Cao, and Z. A. Xu, Phys. Rev. B **82**, 054518 (2010).

[40] C. C. Homes, M. N. Ali, and R. J. Cava, Phys. Rev. B **92**, 161109 (2015).

[41] For clarity, we have outlined the modeling procedure that goes in several stages with one particular type of excitation being accounted for at each stage. Alternatively, one may use the approach in which the parameters of all the processes are calculated at once with the best overall fit. The results are very much the same—some caution is only required with the

low-frequency mode where the noise is stronger than elsewhere, leading to somewhat bigger uncertainty for its parameters.

[42] J. A. Holy, K. C. Woo, M. V. Klein, and F. C. Brown, Phys. Rev. B **16**, 3628 (1977).

[43] The optical conductivity spectrum is expected to change continuously over the second-order phase transition, known to take place near 200 K in $1T$-TiSe$_2$. However, it is also well known that the spectra in the low-temperature CDW phase acquire additional optically active phonon modes above $130\,cm^{-1}$ [23]. These modes, emerging from cell reconstruction and electron charge redistribution within the supercell, do not show in our spectra down to 200 K. This allows us to analyze all the spectra in the same manner and within the same model, appropriate for the high-temperature phase.

[44] U. Fano, Phys. Rev. **124**, 1866 (1961).

[45] N. Dean, J. C. Petersen, D. Fausti, R. I. Tobey, S. Kaiser, L. V. Gasparov, H. Berger, and A. Cavalleri, Phys. Rev. Lett. **106**, 016401 (2011).

[46] C. Thomsen, *Topics in Applied Physics: Light Scattering in Solids VI*, edited by M. Cardona and G. Güntherodt (Springer-Verlag, Berlin, 1991), Vol. 68, p. 327.

[47] See Supplemental Material at http://link.aps.org/supplemental/10.1103/PhysRevB.94.075105 for the values of parameters ω_0, S_0, and $1/q_0$, respectively, standing for the frequency, the strength, and the asymmetry of the phonon signal.

[48] See Supplemental Material at http://link.aps.org/supplemental/10.1103/PhysRevB.94.075105 for the decomposition for the imaginary part of the optical conductivity may be found in Sec. SIII.

[49] See Supplemental Material at http://link.aps.org/supplemental/10.1103/PhysRevB.94.075105 for the example of the numerical parameters used for this part of the model. Up to ten terms with frequencies ω_{Lj} above $1000\,cm^{-1}$ were used here to produce very precise fits. The temperature dependence of the interband part of the spectrum is also illustrated.

[50] The error bars are produced by varying the model parameters that apply to modes below $1000\,cm^{-1}$ to the extent of preserving the overall quality of fits shown in Fig. 1.

[51] As with other Lorentz terms, this term has zero contribution to dc conductivity.

[52] J. van Wezel, P. Nahai-Williamson, and S. S. Saxena, Phys. Rev. B **81**, 165109 (2010).

[53] More precise quantification for electrons in the conduction band in $1T$-TiSe$_2$ would require including the effect of the anisotropy in the conduction-band dispersion as well as the fact that the Fermi see for electrons is made of three equivalent pockets.

[54] The argument also holds if one type of carrier is symmetrically spread across several pockets.

[55] W. Brütting, P. H. Nguyen, W. Riess, and G. Paasch, Phys. Rev. B **51**, 9533 (1995).

[56] P. Monceau, Adv. Phys. **61**, 325 (2012).

[57] A. Zettl, G. Grüner, and A. H. Thompson, Phys. Rev. B **26**, 5760 (1982).

[58] M. Grioni, L. Perfetti, C. Rojas, H. Berger, G. Margaritondo, J. Voit, and H. Höchst, J. Electron Spectrosc. Relat. Phenom. **116**, 653 (2001).

[59] L. Perfetti, H. Berger, A. Reginelli, L. Degiorgi, H. Höchst, J. Voit, G. Margaritondo, and M. Grioni, Phys. Rev. Lett. **87**, 216404 (2001).

[60] A. Schwartz, M. Dressel, B. Alavi, A. Blank, S. Dubois, G. Grüner, B. P. Gorshunov, A. A. Volkov, G. V. Kozlov, S. Thieme, L. Degiorgi, and F. Levy. Phys. Rev. B **52**, 5643 (1995).

[61] B. P. Gorshunov, A. A. Volkov, G. V. Kozlovv, L. Degiorgiv, A. Blank, T. Csiba, M. Dressel, Y. Kim, A. Schwartz, and G. Grüner, Phys. Rev. Lett. **73**, 308 (1994).

[62] B. R. Patton and L. J. Sham, Phys. Rev. Lett. **31**, 631 (1973).

[63] R. H. McKenzie, Phys. Rev. B **52**, 16428 (1995).

[64] V. Sadovskii, Zh. Eksp. Teor. Fiz. **77**, 2070 (1979).

[65] A. F. Kusmartseva, B. Sipos, H. Berger, L. Forró, and E. Tutiš, Phys. Rev. Lett. **103**, 236401 (2009).